

Protein Unfolding at Interfaces: Slow Dynamics of α -Helix to β -Sheet Transition

Ananthakrishnan Sethuraman,¹ Ganesh Vedantham,² Taiji Imoto,³ Todd Przybycien,^{2*} Georges Belfort^{1*}

¹Department of Chemical and Biological Engineering, Rensselaer Polytechnic Institute, Troy, New York

²Department of Biomedical Engineering, Carnegie Mellon University, Pittsburgh, Pennsylvania

³Graduate School of Pharmaceutical Sciences, Kyushu University, Fukuoka 812-8582, Japan

ABSTRACT A two-phase sequential dynamic change in the secondary structure of hen egg lysozyme (Lys) adsorbed on solid substrates was observed. The first phase involved fast conversion of α -helix to random/turns (within the first minute or at very low coverage or high substrate wettability) with no perceptible change in β -sheet content. The second phase (1–1200 min), however, involved a relatively slow conversion from α -helix to β -sheet without a noticeable change in random/turns. An important finding of this work is that the concentration of lysozyme in the adsorbed state has a substantial effect on the fractional content of secondary structures. Attenuated total reflection Fourier transform infrared (ATR/FTIR) spectroscopy, along with a newly-developed optimization algorithm for predicting the content of secondary structure motifs, was used to correlate the secondary structure and the amount of adsorbed lysozyme with the surface wettability of six different flat nanoporous substrates. Although three independent variables, surface wettability, solution concentration and time for adsorption, were used to follow the fractional structural changes of lysozyme, the results were all normalized onto a single plot with the amount adsorbed as the universal independent variable. Consequently, lateral interactions among proteins likely drive the transition process. Direct intermolecular force adhesion measurements between lysozyme and different functionalized self-assembled alkane-thiol monolayers confirm that hydrophobic surfaces interact strongly with proteins. The lysozyme-unfolding pathway during early adsorption appears to be similar to that predicted by published molecular modeling results. *Proteins* 2004;56:669–678.

© 2004 Wiley-Liss, Inc.

Key words: protein folding; secondary structure; protein–substrate interactions

INTRODUCTION

Protein folding, unfolding and aggregation in solution are processes that have been recently linked to disease.^{1,2} How proteins behave at interfaces is also of much interest in the medical and non-medical communities. Protein stability during adsorption is critical for medical devices and procedures (catheters, surgical instruments, implants, synthetic joints, dialysis, drug delivery), for the recovery of proteins in bioprocessing (chromatography and

synthetic membrane filtration) and for adhesion in marine environments (fouling of ship surfaces and other marine structures). This is because protein stability affects removal of the protein from a surface, the recovery of active protein after exposure to a surface, the prevention of aggregation of other proteins at the surface, and the possible triggering of other events such as inflammatory or immune responses.

The native structure of a folded protein is dependent on its amino acid sequence and the solution environment in which it is dissolved.^{3,4} Much recent study has been inspired by the fact that slightly denaturing a so-called ordinary globular protein can result over time in the formation of a radically different structure that closely resembles the amyloid and prion aggregates seen in pathological conditions such as Alzheimer's and Creutzfeldt-Jakob diseases.^{5–7} A characteristic property of these insoluble proto fibrils and fibril aggregates is the presence of increased numbers of β -sheets.^{8–11} Apparently, a well-studied globular protein, wild-type lysozyme, “appears incapable of amyloid fibril formation”⁹ *in vivo* and therefore does not easily form β -sheets. Mutagenesis of lysozyme can, however, produce variants that facilitate amyloid fibril formation *in vivo*.^{12,13} Besides mutagenesis, changes in the normal physiological milieu (solvent,^{6,14} pH^{15,16} and temperature¹⁶) as suggested by Anfinsen³ have been used to induce the formation of β -sheet structures. Klein-Seetharaman and coworkers¹⁴ have recently shown that unfolded lysozyme retains a hydrophobic cluster held together mostly by one critical amino acid, tryptophan 62 (Trp⁶²). In the native lysozyme structure, however, this hydrophobic amino acid, Trp⁶², is highly exposed

The Supplementary Materials referred to in this article can be found at <http://www.interscience.wiley.com/jpages/0887-3585/suppmat/index.html>

Ganesh Vedantham's present address is Amgen Inc, 51 University Street, Seattle, WA 98101.

Grant sponsors: US Department of Energy and the National Science Foundation; Grant numbers DE-FG02-90ER14114 and CTS-94-00610.

*Correspondence to: Georges Belfort, Department of Chemical and Biological Engineering, Rensselaer Polytechnic Institute, Troy, NY 12180. Email: belfog@rpi.edu and Todd Przybycien, Department of Biomedical Engineering, Carnegie Mellon University, Pittsburgh, PA 15213. Email: todd@andrew.cmu.edu

Received 15 October 2003; Revised 29 January 2004; Accepted 11 March 2004

Published online 11 June 2004 in Wiley InterScience (www.interscience.wiley.com). DOI: 10.1002/prot.20183

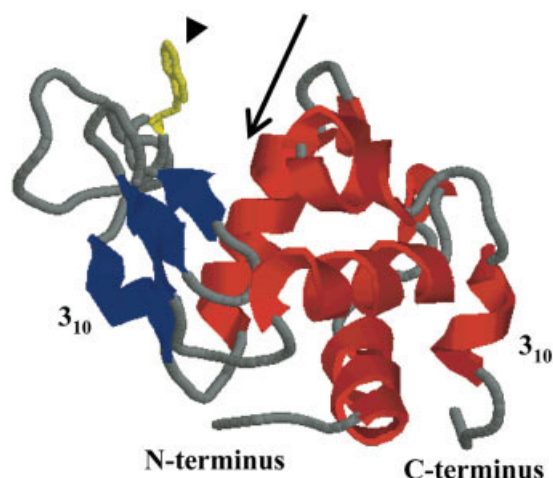


Fig. 1. Ribbon diagram of native hen egg lysozyme (PDB entry 1AZF) comprised of two structural domains, the α -domain (right side of arrow) and the β -domain (left side of arrow). The active site lies between the two domains (arrow). The freely exposed and hydrophobic amino acid Trp⁶² (arrowhead) is replaced by the Gly amino acid for the W62G mutant protein. Figure was generated using Rasmol.

to solvent. The side chain on which it is attached is largely disordered according to the crystal structure¹⁷ and mobile according to nuclear magnetic resonance (NMR) measurements¹⁸ (Fig. 1). Here, we offer a different method of perturbing the native structure of hen egg white lysozyme. By exposing native and mutant (W62G) lysozyme to a series of nanoporous solid substrates characterized by their wettabilities, its native secondary structure can be converted to an alternate structure rich in β -sheets, turns and unordered content. The effects of adsorbed protein concentration on secondary structure were also evaluated. The kinetics of this transition were analyzed and modeled for adsorption of native lysozyme on poly(tetrafluoroethylene) (PTFE).

Despite the large number of studies devoted to protein adsorption, little is known about adsorbed protein activity, orientation and conformation on different polymeric substrates, or with biological (chaperone) substrates.¹⁹ Fibrinogen (340 kDa, tetramer), a large and relatively unstable (with respect to adhesion) protein, when adsorbed onto hydrophobic poly(urethanes), exhibits a secondary structural conformational transition from α -helix to β -sheet.²⁰ For fibronectin, Chittur et al.^{21,22} showed that the ratio of β -sheet to β -turn bands increased with adsorption time, exhibiting a stronger effect on hydrophilic ($-\text{COOH}$) than on hydrophobic ($-\text{CH}_3$) surfaces. Recently, Giacomelli and Norde,²³ using circular dichroism (CD), reported that on adsorption to negatively charged ≈ 100 nm Teflon (copolymer of poly(tetra fluoroethylene and perfluorovinyl ether) colloids from solution, the truncated amyloid β -protein ($\text{A}\beta$ 1–40) exhibited “strong α -helix formation” at low coverage and “a more enriched β -sheet structure” at high coverage. These findings were attributed to protein–substrate and protein–protein interactions, respectively, through ion pairing and hydrophobic interactions.

MATERIALS AND METHODS

Materials

Chicken egg white lysozyme (L6876), acetic acid, Poncau S, sulfosalicylic acid, trichloroacetic acid, sodium chloride, sodium phosphate monobasic, sodium phosphate dibasic and potassium chloride were obtained from Sigma chemical Co. (St. Louis, MO). Regenerated cellulose (RC), polyethersulfone (PES) and poly vinyl pyrrolidone-modified PES (pvp-PES) membranes were gifts from Pall-Fitron (East Hills, NY). Polyvinylidene difluoride (PVDF) and polysulfone (PS) membranes were gifts from Danish Separation Systems, A/S (Nakskov, Denmark) and polytetrafluoroethylene membrane was a gift from W. L. Gore and Associates, Inc. (Elkton, MD).

Infrared Spectral Analysis Algorithm and Measurements

A holistic spectral analysis approach based on ATR/FTIR spectroscopy was used in this study.²⁴ The technique uses amide I band infrared spectra to estimate protein secondary structure. It combines the superposition of reference spectra of pure secondary structural elements with simultaneous aromatic side chain, water vapor and solvent background subtraction. Using a single optimization algorithm, a single mathematical function is defined for protein spectra, permitting all subtractions, normalizations and amide band deconvolution steps to be performed simultaneously. A key element of the technique is the calculation of reference spectra for ordered helix (called α -helix), sheet (called β -sheet), unordered and unordered helix and sheet, and turns structures from a basis set of well-characterized proteins. α -chymotrypsin (bovine pancreas; C7762), concanavalin-A (*Canavalia Ensiformis*; C7275), myoglobin (sperm whale; M7527), papain (papaya latex; P4762) subtilisin (*Bacillus Licheniformis*; 85968) and triosephosphate isomerase (rabbit muscle; T6258) were purchased from Sigma-Aldrich. Lysozyme (chicken egg white; LS002933) and ribonuclease A (bovine pancreas; LS003433) were purchased from Worthington Biochemical Corporation (Lakewood, NJ). These proteins cover a broad range of secondary structural motifs. Structural reference spectra were generated in the amide I ($1600\text{--}1700\text{ cm}^{-1}$) and amide III ($1200\text{--}1300\text{ cm}^{-1}$) bands, both of which are sensitive to protein secondary structure content. Amide I band estimates were significantly better than amide III band estimates, according to our comparison of secondary structure predictions to known secondary structure components from X-ray data; hence, amide I estimates were used here (Supplementary Information).

The estimates for the fractions of turns and unordered helix and random motifs were lumped together because they were the least accurate of the estimates (compared to α -helix and β -sheet). This is possibly because they depend on multiple individual and variable peaks. In other words, α -helix, β -sheet, unordered and unordered helix and sheet, and turns structures depend on 1, 2, 3 and 4 peaks, respectively.

All protein spectra were recorded in their respective aqueous buffer solution.²⁴ The spectra were collected with

a Nicolet Magna 550 Series II FTIR spectrometer (Madison, WI) with a horizontal attenuated total reflection (ATR) accessory (Spectra Tech Inc., Shelton, CT). The ATR accessory was a trapezoidal germanium crystal (7.0×1.0 cm) with ends cut to 45° mounted onto a sample trough, generating 12 internal reflections. The spectrometer was equipped with a liquid nitrogen-cooled mercury cadmium telluride detector. To reduce the contributions of water vapor and carbon dioxide, the IR system was continuously purged with air from a FTIR purge gas generator (Model 74-45, Balston, Inc., Haverhill, MA) at 30 standard cubic feet per minute and supplemented with nitrogen gas from the vent of a liquid nitrogen tank. To obtain protein solution and corresponding buffer background spectra, approximately 250 μ L of each solution was spread evenly to completely cover the germanium crystal. The crystal was then sealed with parafilm to minimize evaporation during acquisition. For generation of the reference spectra, protein concentrations above 20 mg/mL ensured that less than 2% of the FTIR signal derived from molecules adsorbed to the germanium crystal. This assumes a worst-case scenario of monolayer coverage attained by random sequential adsorption with a jamming limit of 55%. All ATR-corrected spectra were collected in the 1000–4000 cm^{-1} range as sets of 1024 time-averaged, double-sided interferograms with Happ-Genzel apodization. Spectral resolution was set at 2 cm^{-1} with a gain of eight and an aperture of 40. After each experiment, the exposed surface of the germanium crystal was cleaned using a five-step process²⁴: (1) rinsing with deionized (DI) water, (2) soaking in a 1% (w/w) sodium dodecyl sulfate (SDS) solution for 10 min, (3) rinsing thoroughly with DI water, (4) rinsing thoroughly with a 50% (w/w) aqueous ethanol solution and (5) drying with compressed air filtered through cotton to remove oils and particulates. Amide I band signal-to-noise (S/N) ratios varied from 804 to 150, whereas amide III band S/N ratios varied from 120 to 20. Amide band S/N ratios were calculated as 2.5 times the maximum intensity of the background-subtracted band divided by three times the standard deviation of the intensity between 1850 and 2200 cm^{-1} . Spectra taken of the cleaned crystal surface did not show any protein adsorbed on the surface.

Protein Adsorption Experiments

Prior to static adsorption, each porous substrate (membrane) was thoroughly rinsed in DI water followed by a mixture of 50% (v/v) ethanol in DI water. The protein solutions were filtered through a 0.22 μ m microfiltration membrane (express PES; Millipore Corp, Bedford, MA) to remove large protein aggregates from solution prior to adsorption.²⁵ Then, static adsorption measurements were conducted by immersing the substrates in 50 mL of protein solution containing 16 mg/mL: in 50 mM phosphate buffer saline (PBS) (150 mM NaCl) at pH 7.4 and allowed to incubate at 25°C for 300 min. Analyses of the irreversibly adsorbed lysozyme were performed by rinsing membranes with the starting buffer and using ATR/FTIR. For the kinetic experiments, washing of the PTFE substrates and the adsorption procedure were similar to the procedures

described above. Substrates were immersed in the protein solution for time, $t = 0, 1, 2, 4, 6, 8, 10, 30, 75, 100, 150, 200, 300, 450, 600, 800, 1000$ and 1200 min, and then analyzed using ATR/FTIR. All buffers were filtered through 0.22 μ m filters before use.

Contact Angle

A captive air bubble was placed under a membrane substrate, both of which were submerged in water, and multiple contact angle values (at least five) were measured using an optical system (SIT camera, SIT66, Dage-MTI, Michigan, IN) converted to a video display. Average values of the contact angles were obtained using more than five different bubbles at different locations on the membrane surface. Additional details can be found in Pieracci et al. (2000).²⁶ Corrections of the contact angles for roughness were obtained using the methods of Taniguchi et al.^{27,28}

Dye Binding Analysis

For dye binding analysis,²⁹ membranes with adsorbed lysozyme were immersed for 1 h in a solution of Ponceau S (20 g/L, in water with 30% (w/v) trichloroacetic acid and 30% (w/v) sulfosalicylic acid), then washed three times with water, immersed for 1 h in 5% (v/v) acetic acid and again washed three times. Then the protein–dye complex was qualitatively eluted with 3 mL of 100 mM NaOH solution (1 h). The membranes were removed, the solutions were neutralized by the addition of 50 mL of 6M HCl, and the absorbance of the red solutions was measured at 515 nm. See Ulbricht et al.²⁹ for additional details.

Kinetic Model

Eqs. (2–4) were solved numerically using the Runge–Kutta method. The initial values of $\phi_{\alpha 0}$, ϕ_{I0} and $\phi_{\beta 0}$ were 0.22, 0.71 and 0.07 respectively. The kinetic model was fit to the experimental data by using least squares fit.

RESULTS AND DISCUSSION

ATR/FTIR Measurements of Lysozyme Secondary Structure on Polymeric Substrates

Hen egg white lysozyme is composed of two structural domains, an α -domain consisting of four α -helices and a C-terminal 3_{10} helix, and a β -domain consisting of a triple-stranded antiparallel β -sheet, a 3_{10} helix and a long loop (Fig. 1). A short double-stranded antiparallel β -sheet links the two domains, as does one of the four disulfide bridges. The active site lies between the two domains. The protein is known to be structurally robust in solution.³⁰ The secondary structure components of lysozyme in PBS buffer, such as α -helices, β -sheets, turns and unordered structures, as determined using ATR/FTIR²⁴ are 0.40, 0.07, 0.40 and 0.13, respectively. The values determined using X-ray³¹ are 0.46, 0.07, 0.42 and 0.05, respectively. Thus, for wild-type lysozyme in free solution, the α -helix content is approximately 40% (by ATR/FTIR), and the β -sheet content is about 7%. Lysozyme has a low dipole moment and approaches the surface in a random orientation³² compared to proteins with large dipole moments such as ribonuclease A, which adsorb in a preferred

TABLE I. Description and Properties of the Nanoporous Substrates (Membranes)

Nanoporous Substrates (Membrane)	Symbol	MWCO ^a (kDa)	Contact Angle (θ) ^b	Wettability Cos (θ)
Poly(tetrafluoroethylene)	PTFE	unknown	120 ± 3	-0.499 ± 0.045
Poly(vinylidene difluoride)	PVDF	20	76 ± 2	0.243 ± 0.033
Poly(sulfone)	PS	20	70 ± 2	0.343 ± 0.033
Poly(ether sulfone)	PES	10	55 ± 2	0.574 ± 0.028
Poly(vinyl pyrrolidinone)-poly(ether sulfone)	pvp-PES	10	48 ± 2	0.669 ± 0.026
Regenerated cellulose	RC	10	27 ± 2	0.891 ± 0.016

^aMWCO - Molecular weight cut off is defined as that molecular weight (in kDa) of a dissolved solute for which 90% of its mass is retained by a membrane during ultrafiltration.

^bSessile captive air bubble contact angle. Atomic force microscope measurements, and a zig-zag model of the surface were used to correct for roughness effects according to Taniguchi et al.^{27,28} Contact angle values are reported as the mean \pm standard deviation of 10 measurements.

orientation.¹⁹ In order to probe the secondary structural changes of adsorbed lysozyme, a series of synthetic polymeric nanoporous substrates was selected as adsorbents (Table I). Following the procedure of Sigal et al.,³³ we used $\cos \theta$ as a measure of the wettability of the substrates, where θ is the captive bubble sessile contact angle between air and the different substrates in water and is corrected for the roughness of the different substrates.^{27,28} Since the usual method of assessing secondary structure in aqueous solution, circular dichroism, is not easily adaptable to adsorbed proteins on solid substrates in aqueous solution, we have used a quantitative approach based on amide I band ATR/FTIR spectroscopy.²⁴ In order to estimate the secondary structure contents of unknown adsorbed lysozyme samples, a simultaneous background subtraction and constrained superposition, or 'holistic' algorithm, based on a set of amide I band reference spectra corresponding to homogeneous secondary structure elements, was used. The mean peak positions for Gaussian-Lorentzian band shapes corresponding to these reference spectra and structural motifs are as follows: α -helix (1652 cm^{-1}), β -sheet (1693 and 1633 cm^{-1}), unordered and unordered helix (1672 , 1648 and 1620 cm^{-1}) and turn structures (1720 , 1668 , 1630 and 1617 cm^{-1}) [Fig. 2(a)]. The deconvoluted spectra for each of these four structural components are easily distinguishable. The dominant peaks for the β -sheet motifs at approximately 1693 cm^{-1} and 1633 cm^{-1} are commonly observed experimentally.³⁴ It is possible that intermolecular protein contacts could lead to a β -sheet-like motif observed at approximately 1622 cm^{-1} . The amide I band did not significantly overlap the bands from the substrates [Fig. 2(b)]. Concentration and kinetic experiments were all conducted with native lysozyme and PTFE as the substrate. Also included in this article is a comparison of the raw spectra for the amide I region for lysozyme in solution and adsorbed on each of the six different substrates [Fig. 2(c)].

In order to show the variation of the secondary structure predictions, the decomposed spectra (variations of α -helix and β -sheet content) for the adsorbed lysozyme on different surfaces, at different times and at varying solution concentrations are shown in Figure 3. The smooth decrease in α -helical peak and the concomitant smooth

increase in β -sheet content with substrate type, lysozyme concentration and time shows the sensitivity of the amide I decomposition algorithm with these variables.

Lysozyme Structure as a Function of Substrate Wettability

The adsorbed amount of lysozyme, which was estimated using the Ponceau S dye binding technique²⁹ (see Methods), was measured for all the substrates. The amount of lysozyme adsorbed (Γ_{ads} , mg/m^2) after 5 h on each of the surfaces listed above correlated linearly and inversely with surface wettability ($\cos \theta$). Fits of the data are given by $y = ax + b$; with $y \equiv \Gamma_{\text{ads}}$, concentration of adsorbed lysozyme, $x \equiv \cos \theta$, membrane wettability. For native and mutant (W62G) the values were $a = -2.71$ and -2.57 , and $b = 3.68$ and 3.44 with R^2 values of 0.999 and 0.984 , respectively. Thus, the most hydrophobic surface (PTFE) adsorbed the highest amount of lysozyme (approx. three calculated adsorbed layers) while the most wettable surface (RC) adsorbed the least amount of lysozyme (less than an adsorbed monolayer) during this period. Within the experimental error, the W62G lysozyme mutant follows the behavior of the native lysozyme during adsorption. Next, we correlated the fraction of secondary structure contents of adsorbed lysozyme after 300 min of adsorption on each nanoporous substrate with surface wettability (Fig. 4). The results show a secondary structural conformational transition from α -helix to β -sheet (and turns/random) with decreasing wettability for both native and mutant (contains less helix and more sheet content than the native lysozyme in free solution and hence on the surface). The α -helix content of native and mutant lysozyme dropped from their native structure values of 40% and 33% in solution to 15% and 12%, respectively, when adsorbed onto PTFE for 5 h. Also, a concomitant increase in β -sheet content, from 7% and 12% for the native and mutant protein in free solution to 18% and 19%, respectively, occurred during this period. Not all of the loss in α -helix content was converted to β -sheet structure, since the remaining secondary structural components (random/turns: unordered, unordered helices) also increased from 54% to 67% and 58% to 69% respectively. Notice that for the most hydrophilic material, regenerated cellulose, the

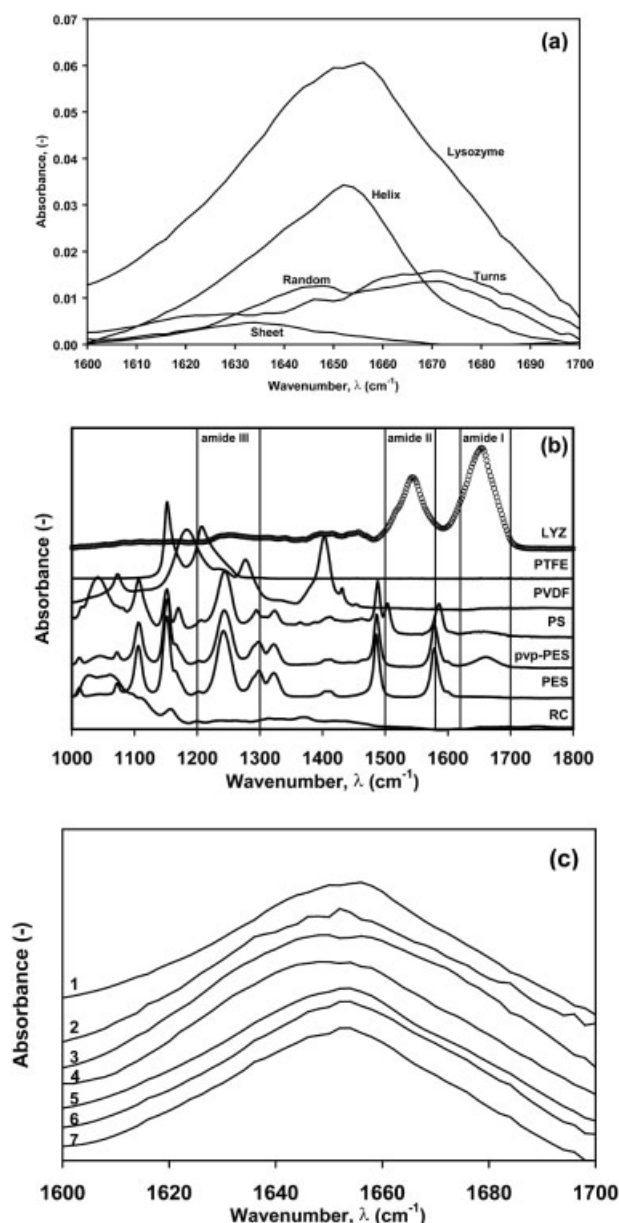


Fig. 2. ATR/FTIR spectroscopy of hen egg lysozyme in PBS and adsorbed from PBS at 25°C. (a) Deconvolution of the amide I band ($1600\text{--}1700\text{ cm}^{-1}$) of the IR spectrum into fractions of secondary structure components: ordered helix (α -helix, 40%); sheet (β -sheet, 7%); random (unordered and unordered helix, 13%) and turns (40%). (b) ATR/FTIR spectra of lysozyme in PBS (\circ) and of the six different substrates (Table I) used in the adsorption experiments in PBS. (c) Superimposed ATR/FTIR spectra (absorbance scale arbitrary) for lysozyme in free solution (PBS) (#1) and lysozyme adsorbed for 300 min from PBS on six different surfaces (PTFE, PVDF, PS, PES, pvp-PES and RC, #2–7, respectively; see Table I for symbols). The lysozyme concentration was 16 mg/mL in PBS at 25°C for all experiments.

secondary structural content of adsorbed native and mutant lysozyme was close to that in free solution (six arrows in Fig. 4), and thus lysozyme was not strongly perturbed from its native structure. Since the highly critical amino acid, Trp⁶², in the native molecule is both hydrophobic and freely accessible to solvent and hence to substrate (Fig. 1),

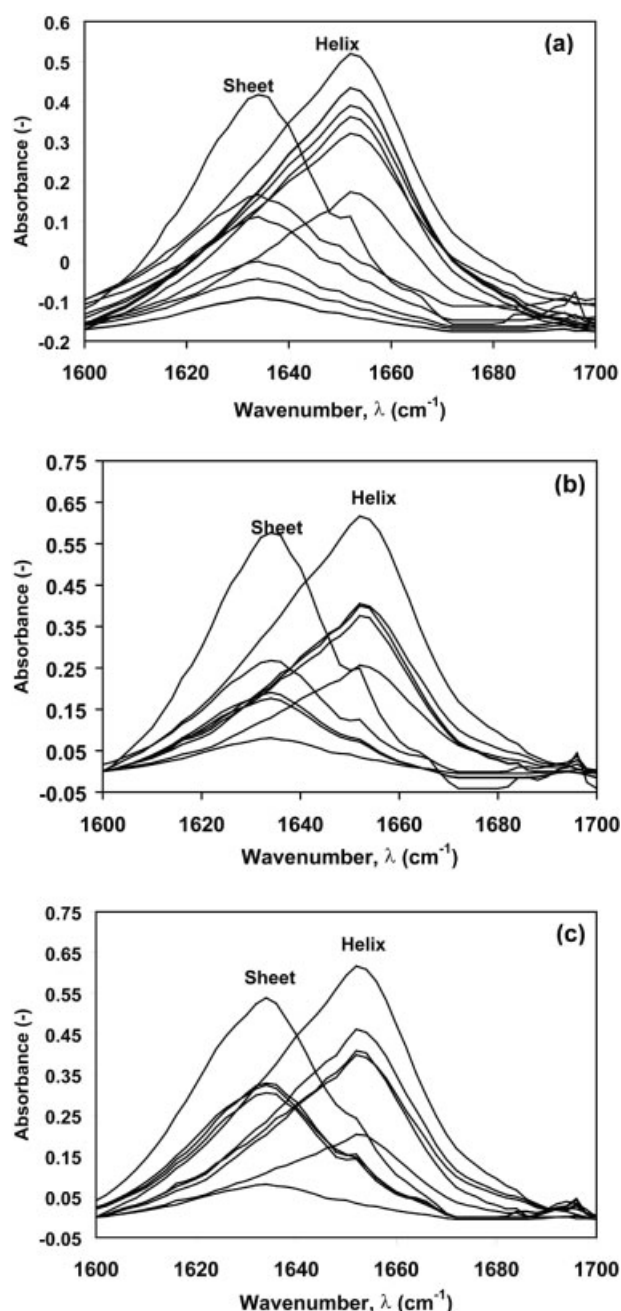


Fig. 3. Secondary structure predictions using our optimization algorithm from the decomposed ATR/FTIR spectra of hen egg lysozyme in PBS and adsorbed from PBS at 25°C. Variation of the fractional helix (1652 cm^{-1}) and sheet (1633 cm^{-1}) components for native (in free solution) and adsorbed lysozyme in PBS as a function of (a) surface substrate type (in order PTFE, PVDF, PS, PES, pvp-PES, & RC and $\text{Lys}_{\text{free solution}}$, decreasing for sheet from the highest spectra and increasing for helix from the lowest spectra) for 300 min adsorption; (b) duration of lysozyme adsorption (in order 600, 150, 30, & 1 min and $\text{Lys}_{\text{free solution}}$ decreasing for sheet from the highest spectra and increasing for helix from the lowest spectra) on PTFE at 16 mg/mL; and (c) lysozyme solution concentration in the solution (in order 16, 8, 4, & 2 mg/mL and $\text{Lys}_{\text{free solution}}$ decreasing for sheet from the highest spectra and increasing for helix from the lowest spectra) for 300 min and on PTFE.

it was tempting to speculate that this amino acid was attracted by hydrophobic interactions to the apolar substrates, causing perturbation of the lysozyme molecule and

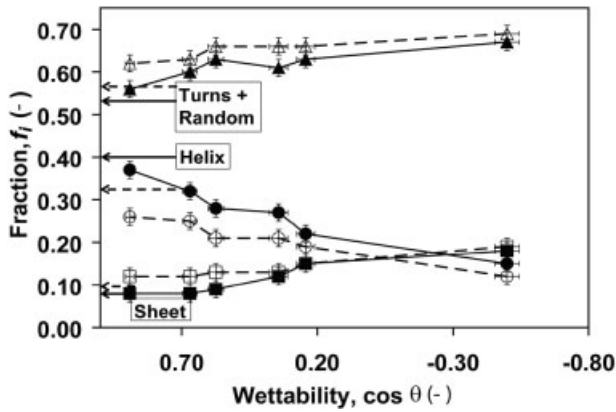


Fig. 4. Fraction of secondary structure components, f_i , of adsorbed native (full symbols) and mutant (W62G, open symbols) lysozyme versus wettability ($\cos \theta$) of the nanoporous substrates. Ordered helix (α -helix, \bullet , \circ); sheet (β -sheet, \blacksquare , \square) and random/turns (unordered, unordered helix and turns, \blacktriangle , \triangle) for lysozyme adsorbed onto six nanoporous substrates in PBS buffer at pH 7.4 and 25°C for 300 min. The six horizontal full and dashed arrows identify the fractional structural components in free solution for the native and W62G mutant, respectively.

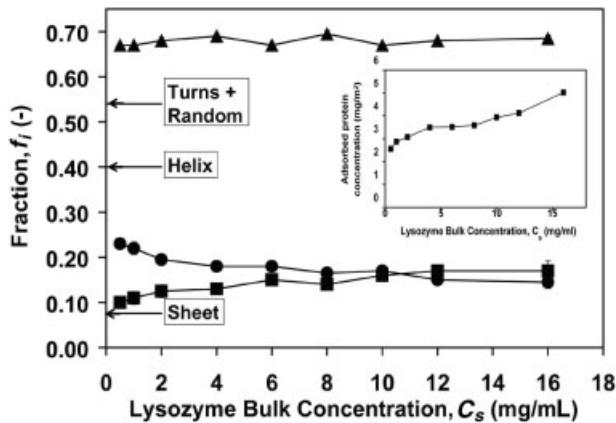


Fig. 5. Fraction of secondary structure components of adsorbed native lysozyme versus initial concentration of native lysozyme in free solution. Ordered helix (α -helix, \bullet); sheet (β -sheet, \blacksquare) and random/turns (unordered, unordered helix and turns, \blacktriangle) for lysozyme adsorbed onto PTFE substrate in PBS buffer at pH 7.4 and 25°C for 300 min. The three horizontal full arrows identify the fractional structural components in free solution for the native lysozyme, respectively. Insert: adsorption isotherm.

possibly increased loss of secondary structure and increased amount adsorbed over that observed with the Gly⁶² mutant. Similar slopes for Γ_{ads} versus $\cos \theta$ for the native and mutant do not support this speculation.

Lysozyme Structure as a Function of Bulk Concentration

The data in Figure 5 show the effect of changing the initial feed concentration, C_s , during adsorption of native lysozyme onto PTFE for 300 min. Again there appears to be an α -helix-to- β -sheet transition with increasing C_s . The adsorption isotherm, shown in the insert of Figure 5, exhibits multilayer-type adsorption, especially at $C_s \geq 8$ mg/mL and at adsorbed amount $\Gamma_{\text{ads}} \geq 3.7$ mg/m².

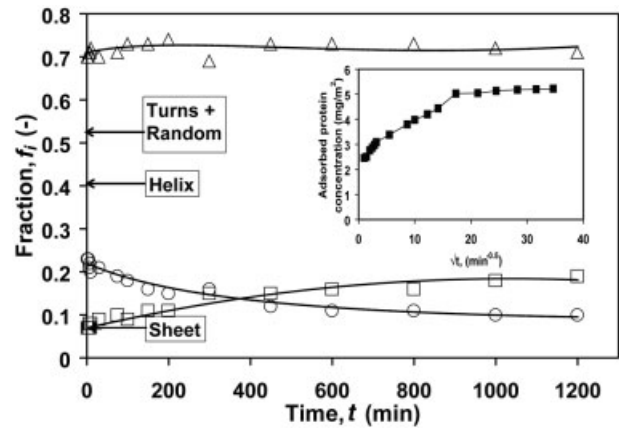


Fig. 6. Fraction of secondary structure components of adsorbed native lysozyme versus time. Ordered helix (α -helix, \circ); sheet (β -sheet, \square) and random/turns (unordered, unordered helix and turns, \triangle) for lysozyme adsorbed onto PTFE substrate in PBS buffer at pH 7.4 and 25°C for 300 min. The three horizontal full arrows identify the fractional structural components in free solution for the native lysozyme. The three solid lines are the model fits and use the initial time points of each period as a starting point. The rate constants for the best fit were $k_1 = 1.22 \times 10^{-3}t + 0.42$; $k_{-1} = 9.95 \times 10^{-5}t + 0.13$; $k_2 = -2.95 \times 10^{-7}t + 3.06 \times 10^{-4}$; and $R^2 = 0.988$. Insert: adsorption kinetics.

Secondary Structure Transition Kinetics on PTFE Substrate

A comparison of the transitional kinetics of the secondary structure components of native lysozyme is presented in Figure 6, along with a fit of the following kinetic model:



where

$$\phi'_{\alpha t} = -k_{1t}\phi_{\alpha} + k_{-1t}\phi_I \quad \phi_{\alpha}(t=0) = \phi_{\alpha 0} \quad (2)$$

$$\phi'_{It} = k_{1t}\phi_{\alpha} - (k_{-1t} + k_{2t})\phi_I \quad \phi_I(t=0) = \phi_{I0} \quad (3)$$

$$\phi'_{\beta t} = k_{2t}\phi_I \quad \phi_{\beta}(t=0) = \phi_{\beta 0} \quad (4)$$

where the rate constant, $k_{it} = a_i t + b_i$ with $i = 1, -1$ and 2, are assumed to be linearly time-dependent and a_i and b_i are constants obtained from the fit. The values k_1 , k_{-1} and k_2 are rate constants for the loss of fractional α -helix (α), the gain of fractional α -helix from intermediate (I) and the loss of intermediate or the formation of β -sheet (β), respectively. The variables designated by ϕ_i are the first differentials of the fractional concentrations ϕ_i with respect to time, t . The initial concentration of each species is represented by ϕ_{i0} . The intermediate fractional concentration ϕ_I is assumed to be equal to the total of the fractional concentrations of random and turns. This boundary value problem [eqs. (2–4)] was solved numerically and is displayed in Figure 6 with the data. Details of the structural changes during the first minute were difficult to observe due to the low amount of adsorbed protein on the surface (low S/N ratio; see insert in Fig. 6). However, after one minute, the fractional α -helix content dropped precipi-

tously, from 0.4 to 0.23 or 43%, while the fractional intermediate (random and turns) content had increased by a similar amount, from 0.53 to 0.70 or 32%, and the β -sheet fractional content had not perceptibly changed (remained at 0.07). The values of the rate constants, k_1 , k_{-1} and k_2 from the model are presented in the legend to Figure 6 as a function of time. Initially ($t = 0$), k_1 was approximately 3 and 1400 times larger than k_{-1} and k_2 , respectively. After 1000 min, k_1 was approximately 7 and 150,000 times larger than k_{-1} and k_2 , respectively. The value of k_1 increases about four times during the time-span of the run, k_{-1} nearly doubles in value and k_2 decreases with time during the 1200 min. The model fits the data extremely well ($R^2 = 0.998$). The amount of lysozyme adsorbed on PTFE with the square root of time suggests three linear diffusion regimes (insert to Fig. 6): short (0–30 min.), intermediate (30–300 min.) and long (300–1200 min.).

Discussion

As is well-known from the modeling and experimental literature, the helix-coil transition ($\alpha \rightarrow I$) for small peptides in solution is very fast, on the order of 20–180 ns,^{35–39} while the folding and unfolding of β -hairpins take about 6 μ s.³⁸ According to Williams et al.,³⁶ “the characteristic time-scale of helix formation would appear to be some 3 orders of magnitude faster than the characteristic time-scale of intra-molecular tertiary contact formation [in free solution].” Restraining a protein on a surface should slow or restrict the formation rate of β -sheet structures, as observed here. Thus, during the adsorption of native lysozyme on a hydrophobic PTFE surface, (i) a large fraction of the α -helices transform into turns and random structures within the first minute with minimum β -sheet formation; (ii) after the first minute, there is a direct slow transition from α -helix to β -sheet and (iii) the fractions of turns and random secondary structures remain relatively constant after the first min. (1–1200 min.).

Since the extent of structural perturbation also corresponds to the amount adsorbed, clearly, for lysozyme, the structural perturbation is the direct result of interaction with the hydrophobic surface, lateral interactions between adjacent lysozyme molecules on the surface or both. To normalize the results, the structural fractional components, f_i , are plotted against the adsorbed native lysozyme concentration Γ_{ads} in Figure 7 for (i) six different surfaces and hence wettabilities (on each substrate after 300 min); (ii) nine different lysozyme bulk concentrations, C_s , (on PTFE for 300 min) and (iii) 17 different time points (on PTFE at 16 mg/mL). As Γ_{ads} increases, a secondary structural conformational transition from α -helix to β -sheet (and turns/random) is observed, confirming the importance of lateral interactions between adsorbed proteins. For the loss of helices, the three data sets appear to follow the same trends. For adsorption onto the hydrophobic PTFE (solid and diagonal lined symbols), most of the helix loss is converted to β -sheets, while for the six different substrates (open symbols), some of the helix loss is also transformed to turns and random structures, especially on the more wettable surfaces. Whether the surface concentra-

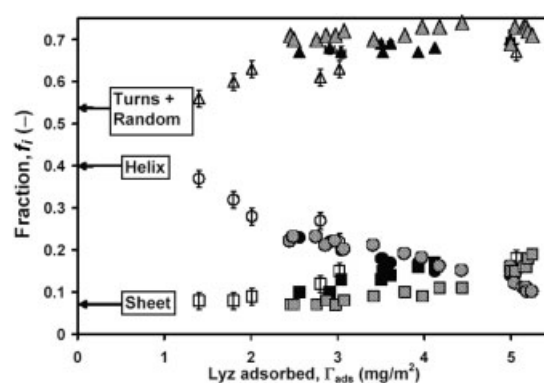


Fig. 7. Fraction of secondary structure components of adsorbed native lysozyme versus amount of lysozyme adsorbed for (i) six different surfaces and hence wettabilities (on each substrate after 300 min) (\circ , \square , \triangle), and (ii) nine different lysozyme bulk concentrations, C_s , (on PTFE for 300 min) (\bullet , \blacksquare , \blacktriangle), and (iii) 17 different time points (on PTFE at 16 mg/mL) (\odot , \boxtimes , Δ). Ordered helix (α -helix, \circ , \bullet , \odot), sheet (β -sheet, \square , \blacksquare , \boxtimes) and random/turns (unordered, unordered helix and turns, \triangle , \blacktriangle , Δ). Three horizontal full arrows identify the fractional structural components in free solution for the native lysozyme.

tion is increased through increasing substrate hydrophobicity (decreasing wettability), by increasing the initial solution concentration or by increasing the adsorption time on a hydrophobic substrate, the results are similar. In previous work with lysozyme adsorption on hydrophobic chromatography media using the same deconvolution method with Raman spectroscopy, β -sheet content increased on adsorption, and greater loading corresponded to greater increase in β -sheet content.⁴⁰ Giacomelli and Norde²³ have reported a similar result (α -helix to β -sheet transition) with increased loading for a truncated amyloid β -peptide adsorbed onto 100 nm negatively charged PTFE particles using CD.

Direct intermolecular adhesion measurements between lysozyme and different functionalized self-assembled alkanethiol monolayers, using a modified atomic force microscope cantilever, show that ‘pull-off’ or adhesive forces are substantial ($\approx 10 \pm 3$ mN/m) between lysozyme and apolar (hydrophobic) surfaces ($-\text{CH}_3$, $-\text{OPh}$, $-\text{CN}$, $-\text{OCH}_3$ and $-\text{CF}_3$), low ($\approx 2.3 \pm 0.4$ mN/m) between lysozyme and wettable (hydrophilic) surfaces ($-\text{OH}$, $-\text{CONH}_2$ and $-\text{ethylene glycol}$) and exceedingly low between lysozyme and lysozyme ($\approx 0.5 \pm 0.2$ mN/m).⁴¹ The lateral interactions among native Lys molecules in free solution is minimal, as their native secondary structure does not change over >70 h (data not shown). Thus, exposed, freely-available hydrophobic amino acids such as Trp⁶² in lysozyme could interact with apolar surfaces through hydrophobic interactions and help explain the increased amount of lysozyme adsorbed onto apolar surfaces. The surface roughness has little influence on disturbing protein structure because the roughness length scale is an order of magnitude larger than the protein dimensions.^{42,43}

Recent experimental and theoretical work on the folding⁴⁴ and unfolding⁴⁵ of lysozyme may provide insight on how this protein behaves during the adsorption process. Their folding pathways to and from the native structure

TABLE II. Fractional Secondary Structural Content in α - and β -domains of Hen Egg Lysozyme^a

Domain	Helix		Sheet		Turns		Random	
	Residues	%	Residues	%	Residues	%	Residues	%
α	54	42	0	0	18	14	5	4
β	5	4	9	7	36	28	2	1
Total	59	46	9	7	54	42	7	5

^aAll secondary structure assignments were made using the STRIDE algorithm of Frishman and Argos.³¹

are likely different.⁴⁵ Using a new molecular dynamics procedure in which water molecules are artificially inserted into cavities during unfolding, Williams et al.⁴⁵ have shown that the first rate-limiting transition corresponds to the “disruption of the tertiary contacts within the protein, which decouples its domains” and that “subsequently, the helical domain slowly loses its compactness and the helices fluctuate rapidly. The protein then adopts a ‘molten globule-like’ structure in which the native β -sheet is essentially intact.” Referring to the secondary structure composition of the α - and β -domains shown in Table II, we first observe an immediate loss of helix during the first minute of adsorption (or at very low surface concentrations) while maintaining the sheet structure. This loss in α -helix content (about 45%) is most likely from the α -domain that has over 90% of the helix content of native lysozyme. After the first minute, we observe that all of the β -sheet content in the β -domain remains, while about half of the α -helix content in the α -domain remains (Fig. 1). This is similar to the result predicted by Williams et al.,⁴⁵ which they state as “only some of the secondary structure is completely stable” (in their case 90% of the β -sheet and 40% of the helix). We then observe a slow α -helix to β -sheet transition over the next 1200 min with the β -sheet content doubling during this period. Since the β -domain comprises all of the β -sheet content of native lysozyme, the β -sheet content can only increase above its native value via a secondary structure transition. In our case, the observed α -helix transition could have come from both domains (about 9% and the rest from the β - and α -domains, respectively). Thus, our early results are consistent with the predicted behavior from molecular modeling, implying that lysozyme unfolding during adsorption occurs along a pathway similar to that predicted by Williams et al.⁴⁵

Since protein aggregates formed on a surface could desorb and form seeds for further aggregation and adsorption,⁴⁶ it is instructive to determine what condition the lysozyme was in (native or aggregated) during the adsorption process on the Teflon substrate. This can be estimated from the diffusion coefficient, D_{LYS} (cm^2/s), of lysozyme in buffer from the kinetic data. Here we plot the amount adsorbed, Γ (mg/m^2) versus $(t)^{0.5}$ according to the expression⁴⁷

$$\Gamma(t) = (2/(\pi)^{0.5})C_S(D_{\text{LYS}}t)^{0.5} \quad (5)$$

where C_S (mg/L) is the concentration of lysozyme in solution (insert to Fig. 6). For the early data [$(t)^{0.5} < 17.32 \text{ min}^{0.5}$], $D_{\text{LYS}} \approx 11.3 \pm 0.2 \times 10^{-7} \text{ cm}^2/\text{s}$, while for longer

times, $D_{\text{LYS}} \approx 0.80 \pm 0.1 \times 10^{-7} \text{ cm}^2/\text{s}$ or 14 times slower. Squire and Himmel⁴⁸ report that in free solution $D_{\text{LYS}} \approx 11.3 \times 10^{-7} \text{ cm}^2/\text{s}$, the same value as the early data value (within error) and close to the measured diffusion coefficient, $D_{\text{LYS}} \approx 10.4 \pm 0.2 \times 10^{-7} \text{ cm}^2/\text{s}$ at the same lysozyme concentration, determined using light scattering.⁴⁹

From the sigmoid Brunauer-Emmett-Teller (BET)-type isotherm for lysozyme on Teflon (insert to Fig. 5), monolayer coverage likely occurred at $\Gamma \approx 3.6 \text{ mg}/\text{m}^2$ (at $C_S \approx 3.5 \times 10^3 \text{ mg}/\text{L}$ from isotherm plot), with multi-layer coverage at higher values. Returning to the kinetic data, it appears that mostly native protein (and not many aggregates) adsorbed onto the Teflon substrate for the first 290 min and until the adsorbed amount on the surface reached $\Gamma \approx 5 \text{ mg}/\text{m}^2$. Even after the monolayer was completed at $\Gamma \approx 3.6 \text{ mg}/\text{m}^2$, monomers continued to adsorb onto the surface until $\Gamma \approx 5 \text{ mg}/\text{m}^2$. Clearly, protein-protein interactions and subsequent conformational changes occurred when the proteins were associated with the surface and intensified as the adsorbate concentration increased.

CONCLUSIONS

These results demonstrate that, besides mutagenesis and variations in pH and temperature, solid substrates characterized by their wettability can perturb the contents of the native secondary structure of hen egg lysozyme and produce alternate structures rich in β -sheets. This is affected by the surface chemistry of the solid substrate due to increased lateral interactions resulting from the increased adsorbed amount and not in our case by surface roughness. The kinetics of these structural changes for adsorbed lysozyme are orders of magnitude slower than those determined during folding in free solution. This is likely due to restricted internal rearrangements within an already folded but structurally disturbed protein. After a fast initial loss in fractional α -helix content, there appears to be a slow conversion of α -helix to β -sheet structural content over a relatively long time (1–1200 min.). Clearly, even an ordinary globular protein such as lysozyme can change its secondary structure by adsorbing onto a substrate for a few hours. The less wettable or more hydrophobic the substrate, the greater this perturbation in secondary structure will be. For adsorbed lysozyme, the unfolding pathway during the first minute appears to follow that predicted by molecular modeling.⁴⁵

From these studies, one can conclude that lysozyme molecules are not adsorbed from solution in the aggre-

gated state, and that they are relatively stable in their native state and likely interact with themselves in the adsorbed state. Koehler et al.,^{50, 51} using the surface forces apparatus with freely adsorbed (not covalently bound) lysozyme, showed that adsorbed lysozyme-lysozyme interactions are much less evident on hydrophilic than on hydrophobic surfaces. Others have shown that adsorbed lysozyme exhibits ordered two-dimensional arrays on graphite,⁵² while on mica it forms two-dimensional structures at low and aggregates at high surface concentrations.^{53, 54} We have demonstrated, based on the fact that lysozyme changes its conformational state as a function of adsorbate concentration (universal plot, Fig. 7), lateral interactions among lysozyme molecules drive the process. Strong evidence is presented here suggesting that protein aggregation occurs on the less wettable surfaces. That this adsorption process might induce aggregation and amyloid formation may bear great importance for healthcare and medical treatments. Although the extent of protein aggregation on the different surfaces was not quantitatively measured (due to the difficulty of distinguishing the low-frequency antiparallel β -sheet peak at $\approx 1622\text{ cm}^{-1}$ from the overlapping H_2O peak and substrate peaks), such measurements are accessible using D_2O . This peak (1622 cm^{-1}) has been attributed to intermolecular β -sheet formation and hence has been used as a measure of aggregation.^{55–60} The optimization algorithm (used with ATR/FTIR) subsumes this peak as turns. However, future work will investigate the extent of protein aggregation on surfaces by measuring the $\approx 1622\text{ cm}^{-1}$ peak for the adsorbed protein in D_2O buffers. Peak fitting and second derivative methods will be used to deconvolute the protein FTIR spectra measured in D_2O buffers.

The approach presented here provides an interesting model system to study the internal structural pathways in structurally restricted (adsorbed) proteins as opposed to those of proteins in free solution³⁶ or to folding pathways of proteins in the denatured state.³⁸ An understanding of how neighboring proteins interact and how this affects their secondary structure is clearly necessary. Perhaps molecular modeling will be of use here.⁶¹

ACKNOWLEDGMENTS

We thank Ole J. Olsen of Danish Separation Systems A/S (now Alpha Laval AB), Bill Short and Monty Carlisle of W. L. Gore and Assoc, Inc. and Barry Breslau and Michael Heath of Pall-Filtron Corp. for donating synthetic membranes and Arthur Hewig for helping with the FTIR technique. We acknowledge the support of the US Department of Energy (Grant No. DE-FG02-90ER14114) and the National Science Foundation (Grant No. CTS-94-00610).

REFERENCES

- Dobson CM. Protein misfolding, evolution and disease. *Trends Biochem Sci* 1999;24:329–332.
- Blakeslee S. In: *Folding proteins, clues to many diseases*. The New York Times, Science Times May 21, 2002; Sect F; pp. F1 & F8.
- Anfinsen CB. Principles that govern the folding of protein chains. *Science* 1973;181:223–230.
- Creighton TE. *Proteins, structures and molecular properties*. New York: W. H. Freeman and Company 1993.
- Sipe JD, Cohen AS. Review: history of the amyloid fibril. *J Struct Biol* 2000;130:88–98.
- Chiti F, Webster P, Taddei N, Clark A, Stefani M, Ramponi G, Dobson CM. Designing conditions for *in vitro* formation of amyloid protofilaments and fibrils. *Proc Natl Acad Sci* 1999;96:3590–3594.
- Fandrich M, Fletcher MA, Dobson CM. Amyloid fibrils from muscle myoglobin. *Nature* 2001;410:165–166.
- Sunde M, Blake CCF. From the globular to the fibrous state: protein structure and structural conversion in amyloid formation. *Quart Revs Biophys* 1998;31:1–39.
- Kelly JW. The alternate conformations of amyloidogenic proteins and their multi-step assembly pathways. *Curr Opin Struct Biol* 1998;8:101–106.
- Rochet J-C, Lansbury Jr PT. Amyloid fibrillogenesis: themes and variations. *Curr Opin Struct Biol* 2000;10:60–68.
- Lansbury Jr. PT. Evolution of amyloid: what normal protein folding may tell us about fibrillogenesis and disease. *Proc Natl Acad Sci* 1999;96:3342–3344.
- Pepys MB, Hawkins PN, Booth DR, Vigushin DM, Tennent GA, Soutar AK, Totty N, Nguyen O, Blake CC, Terry CJ, Feast TG, Zalin AM, Hsuan JJ. Human lysozyme gene mutations cause hereditary systemic amyloidosis. *Nature* 1993;362:553–557.
- Booth DR, Sunde M, Bellotti V, Robinson CV, Hutchinson WL, Fraser PE, Hawkins PN, Dobson CM, Radford SE, Blake CC, Pepys MB. Instability, unfolding and aggregation of human lysozyme variants under lying amyloid fibrillogenesis. *Nature* 1997;385:787–793.
- Klein-Seetharaman J, Oikawa M, Grimshaw SB, Wirmer J, Duchardt E, Ueda T, Imoto T, Smith LJ, Dobson CM, Schwalbe H. Long-range interactions within a nonnative protein. *Science* 2002; 295:1719–1722.
- Zanusso G, Farinazzo A, Fiorini M, Gelati M, Castagna A, Righetti PG, Rizzuto N, Monaco S. pH-dependent prion protein conformation in classical Creutzfeldt-Jakob disease. *J Biol Chem* 2001;276: 40377–40380.
- Chehin R, Iloro I, Marcos MJ, Villar E, Shnyrov VL, Arrondo JL. Thermal and pH-induced conformational changes of a β -sheet protein monitored by infrared spectroscopy. *Biochemistry* 1999;38: 1525–1530.
- Blake CC, Koenig DF, Mair GA, North AC, Phillips DC, Sarma VR. Structure of hen egg-white lysozyme: A three dimensional Fourier synthesis at 2 Å resolution. *Nature* 1965;206:757–761.
- Buck M, Boyd J, Redfield C, MacKenzie DA, Jeenes DJ, Archer DB, Dobson CM. Structural determinants of protein dynamics: analysis of 15N NMR relaxation measurements for main-chain and side-chain nuclei of hen egg white lysozyme. *Biochemistry* 1995;34:4041–4055.
- Lee C-S, Belfort G. Changing activity of ribonuclease A during adsorption: a molecular explanation. *Proc Natl Acad Sci* 1989;86: 8392–8396.
- Lenk TJ, Horbett TA, Ratner BD, Chittur KK. Infrared spectroscopy studies of time-dependent changes in fibrinogen adsorbed to polyurethanes. *Langmuir* 1991;7:1755–1764.
- Chittur KK. Proteins on surfaces: Methodologies for surface preparation and engineering protein function. In: Malmsten M, editor. *Biopolymers at Interfaces*. New York: Dekker; 2003. p 467–496.
- Cheng S-S, Chittur KK, Sukenik CN, Culp LA, Lewandowska K. The conformation of fibronectin on self-assembled monolayers with different surface composition: an FTIR/ATR study. *J Coll Interf Sci* 1994;162:135–143.
- Giacomelli CE, Norde W. Influence of hydrophobic Teflon particles on the structure of amyloid β -peptide. *Biomacromolecules* 2003;4: 1719–1726.
- Vedantham G, Sparks HG, Sane SU, Tzannis S, Przybycien TM. A holistic approach for protein secondary structure estimation from infrared spectra in H_2O solutions. *Anal Biochem* 2000;285:33–49.
- Saksena S, Zydney AL. Influence of protein-protein interactions on bulk mass transport during ultrafiltration. *J Membrane Sci* 1997;125:93–108.
- Pieracci J, Wood DW, Crivello JV, Belfort G. UV-assisted graft polymerization of N-vinyl-2-pyrrolidinone onto poly(ether sulfone) ultrafiltration membranes: comparison of dip versus immersion modification techniques. *Chem of Mat* 2000;12:2123–2133.
- Taniguchi M, Pieracci JP, Belfort G. Effect of undulations on surface energy: a quantitative assessment. *Langmuir* 2001;17: 4312–4315.

28. Taniguchi M, Belfort G. Correcting for surface roughness: advancing and receding contact angles. *Langmuir* 2002;18:6465–6467.
29. Ulbricht M, Matuschewski H, Oechel A, Hicke H-G. Photo-induced graft polymerization surface modifications for the preparation of hydrophilic and low-protein-adsorbing ultrafiltration membranes. *J Mem Sci* 1996;115:31–47.
30. Arai T, Norde W. The behavior of some model proteins at solid-liquid interfaces. 1. Adsorption from single protein solutions. *Coll and surf* 1990;51:1–15.
31. Frishman D, Argos P. Knowledge based protein secondary structure assignment. *Prot: Struct, Func and Gen* 1995;23:566–579.
32. Norde W. Driving forces for protein adsorption at solid surfaces. In: Malmsten M, editor. *Biopolymers at Interfaces*. New York: Dekker; 2003. p 21–44.
33. Sigal M, Mrksich M, Whitesides GM. Effect of surface wettability on the adsorption of proteins and detergents. *J Am Chem Soc* 1998;120:3464–3473.
34. Cooper EA, Knutson K. Physical methods to characterize pharmaceutical proteins. Herron, JN, Jiskoot, W, Crommelin DJA, editors. New York: Crommelin, Plenum Press 1995.
35. Eaton WA, Munoz V, Hagen SJ, Jas GS, Lapidus LJ, Henry ER, Hofrichter J. Fast kinetics and mechanisms in protein folding. *Annu Rev Biophys Biomol Struct* 2000;29:327–359.
36. Williams S, Causgrove TP, Gilmanshin R, Fang KS, Callender RH, Woodruff WH, Dyer RB. Fast events in protein folding: helix melting and formation in a small peptide. *Biochemistry* 1996;35:691–697.
37. Hummer G, Garcia AE, Garde S. Helix nucleation kinetics from molecular simulations in explicit solvent. *Prot: Struct, Func and Gen* 2001;42:77–84.
38. Munoz V, Thompson PA, Hofrichter J, Eaton WA. Folding dynamics and mechanism of beta-hairpin formation. *Nature* 1997;390:196–199.
39. Kauffmann E, Darnton NC, Austin RH, Batt C, Gerwert K. Lifetimes of intermediates in the beta-sheet to alpha-helix transition of beta-lactoglobulin by using a diffusional IR mixer. *Proc Natl Acad Sci* 2001;98:6646–6649.
40. Sane SU, Cramer SM, Przybycien TM. A holistic approach to protein secondary structure characterization using amide I band raman spectroscopy. *J Chrom A* 1999;269:255–272.
41. Sethuraman, Han, Kane and Belfort. Submitted.
42. Denis FA, et al. Protein adsorption on model surfaces with controlled nanotopography and chemistry. *Langmuir* 2002;18:819–828.
43. Han M, Sethuraman A, Kane RS, Belfort G. Nanometer-scale roughness having little effect on the amount or structure of adsorbed protein. *Langmuir* 2003;19:9868–9872.
44. Matagne A, Dobson CM. The folding process of hen lysozyme: a perspective from the 'new view.' *Cell Mol Life Sci* 1998;54:363–371.
45. Williams MA, Thornton JM, Goodfellow JM. Modelling protein unfolding: hen egg-white lysozyme. *Protein Eng* 1997;10:895–903.
46. Tzannis ST, Hrushesky WJM, Wood PA, Przybycien TM. Irreversible inactivation of interleukin-2 in a pump-based delivery environment. *Proc Natl Acad Sci* 1996;93:5460–5465.
47. Amiel C, Sikka M, Schneider JW, Tsao YH, Tirrell M, Mays JW. Adsorption of hydrophilic-hydrophobic block co-polymers on silica from aqueous solutions. *Macromol* 1997;28:3125–3134.
48. Squire PG, Himmel ME. Hydrodynamics and protein hydration. *Arch Biochem Biophys* 1979;196:165–177.
49. Sethuraman and Belfort, Unpublished.
50. Koehler JA, Ulbricht M, Belfort G. Intermolecular forces between proteins and polymer films with relevance to filtration. *Langmuir* 1997;13:4162–4171.
51. Koehler JA, Ulbricht M, Belfort G. Intermolecular forces between a protein and a hydrophilic modified polysulfone film with relevance to filtration. *Langmuir* 2000;16:10419–10427.
52. Haggerty L, Lenhoff AM. Analysis of ordered arrays of adsorbed lysozyme by scanning tunneling microscopy. *Biophys J* 1993;64:886–895.
53. Tilton RD, Blomberg E, Claesson PM. Effect of anionic surfactant on interactions between lysozyme layers adsorbed on mica. *Langmuir* 1993;9:2102–2108.
54. Blomberg E, Claesson PM, Fröberg JC, Tilton RD. Interaction between adsorbed layers of lysozyme studied with the surface force technique. *Langmuir* 1994;10:2325–2334.
55. Zurdo J, Guijarro JL, Jimenez JL, Saibil HR, Dobson CM. Dependence on solution conditions of aggregation and amyloid formation by an SH3 domain. *J Mol Biol* 2001;311:325–340.
56. Sokolowski F, Modler AJ, Masuch R, Zirwer D, Baier M, Lutsch G, Moss DA, Gast K, Naumann D. Formation of critical oligomers is a key event during conformational transition of recombinant syrian hamster prion protein. *J Biol Chem* 2003;278:40481–40492.
57. Kubelka J, Keiderling TA. Differentiation of beta-sheet-forming structures: *ab initio*-based simulations of IR absorption and vibrational CD for model peptide and protein beta-sheets. *J Am Chem Soc* 2001;123:12048–12058.
58. Ismail AA, Mantsch HH, Wong PT. Aggregation of chymotrypsinogen: portrait by infrared spectroscopy. *Biochim Biophys Acta* 1992;1121:183–188.
59. Dong A, Prestrelski SJ, Allison SD, Carpenter JF. Infrared spectroscopic studies of lyophilization- and temperature-induced protein aggregation. *J Pharm Sci* 1995;84:415–424.
60. Militello V, Casarino C, Emanuele A, Giostra A, Pullara F, Leone M. Aggregation kinetics of bovine serum albumin studied by FTIR spectroscopy and light scattering. *Biophys Chem* 2004;107:175–187.
61. DeMarco ML, Daggett V. From conversion to aggregation: protofibril formation of the prion protein. *Proc Natl Acad Sci* 2004;101:2293–2298.